Supporting Information for

Extracellular vesicle refractive index derivation utilizing orthogonal characterization.

Michelle L. Pleet, Sean Cook, Vera A. Tang, Emily Stack, Joanne Lannigan, Ngoc Do, Ellie Wenger, Jean-Luc Fraikin, Steven Jacobson, Jennifer C. Jones, Joshua A. Welsh

Corresponding author: Joshua A. Welsh.
E-mail: joshua.welsh@nih.gov

This PDF file includes:

Contents

1. Materials Methods

A. Reference material preparation. Commercial recombinant EVs (rEVs) (Millipore Sigma, Cat. SAE0193) expressing enhanced green fluorescent protein (EGFP) were resuspended from lyophilization according to manufacturer recommendations in 100 µL deionized water (Sigma Aldrich, Cat. 270733) and reverse pipetted to thoroughly dissolve the pellet.

B. Microfluidic Resistive Pulse Sensing. rEV samples were diluted to a concentration of 1x109 particle mL-1 in DPBS (ThermoFisher Scientific, Cat. 14190144) with 1% Tween 20 (Sigma Aldrich, Cat. P1379) with 240 nm NIST-traceable beads (Thermo Fisher Scientific, 3000 series) at a concentration of 1x109 particles mL-1. Samples were acquired on a Spectradyne nCS1 instrument. The relationship between rEV surface area and fluorescence intensity was acquired on a Spectradyne Arc instrument with rEVs at 1x109 particle mL-1 in DPBS with 1x109 particles mL-1 240 nm NIST-traceable beads. Red FluoSpheres (100 nm Cat. 8801, Lot. 1902792; 200 nm 8810, Lot. 1812162), and silica beads (100 nm, nanoComposix, Cat. SISN100, Lot. GK2461843-03; 200 nm, nanoComposix, Cat. SISN200, Lot. GK2201843-02) were measured at a concentration of 1x109 particles mL with a 269 nm NIST-traceable bead at 1x109 particles mL (Thermo Fisher Scientific, 3000 series) with 1% Tween 20. Samples were processed and outputted into .mat files for downstream analysis using RPSPASS (https://nano.ccr.cancer.gov/rpspass).

C. Flow Cytometry. FCM fluorescence and light scattering settings were optimized and calibrated utilizing FCMPASS (v4.12, https://nano.ccr.cancer.gov/fcmpass). Calibration reference materials, acquisition files, settings, QC plots, and MIFlowCyt and MIFlowCyt-EV reports can be found in Supplementary Information 17-10. RI was derived on an Aurora (Cytek Bioscience) with an enhanced small particle detection (ESP) module with 405 (50 mW), 488 (150 mW), 561 (150 mW), 640 (50 mW) nm lasers. RI derivations were validated using a CytoFLEX S (Beckman Coulter) with 405 (100 mW), 488 (50 mW), 561 (30 mW), 640 nm (50 mW).

D. Statistical analysis & data availability. All data and analysis scripts can be accessed at the repository link: https://doi.org/10.6084/m9.figshare.22009382, flow cytometry files can be found at: https://genboree.org/nano-ui/manuscript/1753349352. Data was analysed in MATLAB (Mathworks Inc, v2022b).

2. Light scatter modelling using Mie theory

The incident electric field can be calculated with the following variables: the electric field amplitude; $E_(0,x)$, the angular frequency; ω, the time; t, the orthonormal basis; $\hat{e}_x$ vector in the direction of the positive x axis, the wave number; $k = 2\pi n/\lambda$, and the wavelength; λ of the incident light in vacuum, in equation 1.

$$E_i = E_{0,x} e^{i(kz-\omega t)} \hat{e}_x \quad [1]$$

Scattering cross section is a hypothetical area describing the probability of light with unit incident irradiance being scattered by a particle. Scatter cross section can be described using the polar angle; ϵ, the azimuthal angle; ϕ, the vector scattering amplitude; X, and the wave number; k, in equation 2.

$$C_{sca} = \int_0^{2\pi} \int_0^{\pi} \frac{|X^2|}{k^2} \sin\theta d\theta d\phi \quad [2]$$

In the FCM$_{\text{PASS}}$ software, ϕ is used to describe circular collection geometries. Circular collection geometries, θ are integrated from $\theta_1 = \theta_0 - \epsilon$ to $\theta_2 = \theta_0 + \epsilon$ with $\phi_1 = \epsilon - f$and $\phi_2 = \epsilon + f$, with f expressed in equation 3.

$$f = \frac{\cos\epsilon - \cos\theta\cos\theta_0}{\sin\theta\sin\theta_0} \quad [3]$$

The number of steps over which θ and ϕ are integrated is 720. For a spherical particle, the vector scattering amplitude X is related to the amplitude scattering matrix elements S_j as shown in equation 4, and shown in Figure S1.

$$X = (S_2\cos\phi)\hat{e}_{||S} + (S_1\sin\phi)\hat{e}_{\perp S} \quad [4]$$

where the basis vector is parallel $\hat{e}_{||S}$ and perpendicular $\hat{e}_{\perp S}$ to the scattering plane, which is defined by the scattering direction $\hat{e}_r$ and the propagation direction of the wave $\hat{e}_z$. The parameters S_1 and S_2 depend on d, n_p, n_m, k, and θ, which are calculated using the Mätzler scripts(1) which are based on the Mie theory formalism of Bohren and Huffman (2). Due to $\hat{e}_{||S}$ and $\hat{e}_{\perp S}$ being orthogonal, $|X^2|$ can be expressed as in equation 5.

$$|X|^2 = |S_2^2|\cos^2\phi + |S_1^2|\sin^2\phi \quad [5]$$

The collection angle at which the Cytek Aurora flow cytometer was modelled at was derived using the FCM$_{\text{PASS}}$ software. Calibrationg was performed using NIST-traceable polystyrene beads with known diameter and refractive index(3). This circular collection half-angle was determined to be 67.5°, shown in Figure S2.

Once the collection half-angle of the flow cytometer had been derived, a refractive index database was generated to allow interpolation of effective scattering cross section and diameter to derive refractive index on a per particle basis. This database

was generated for homogeneous sphere and core-shell models at a wavelength of 405 nm with a surrounding medium refractive index of 1.3431. Core-shell models assumed a shell thickness of 6 nm based on literature of phospholipid bilayer measurements. The range of core and homogeneous sphere refractive indices ranged from 1.3 to 2 in increments of 0.0005. Diameters of 1 to 3000 nm were modelled in 0.1 nm increments.

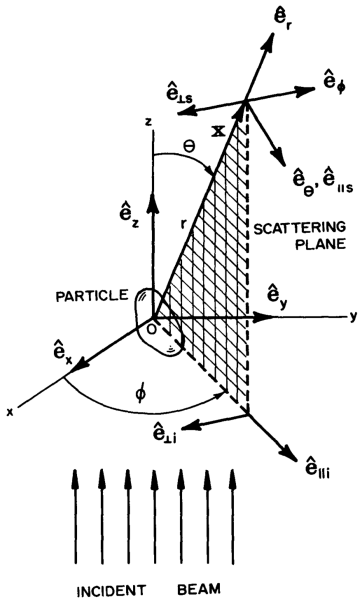

Fig. S1. Modelling scatter planes taken from Bohren and Huffman, 1983, p62

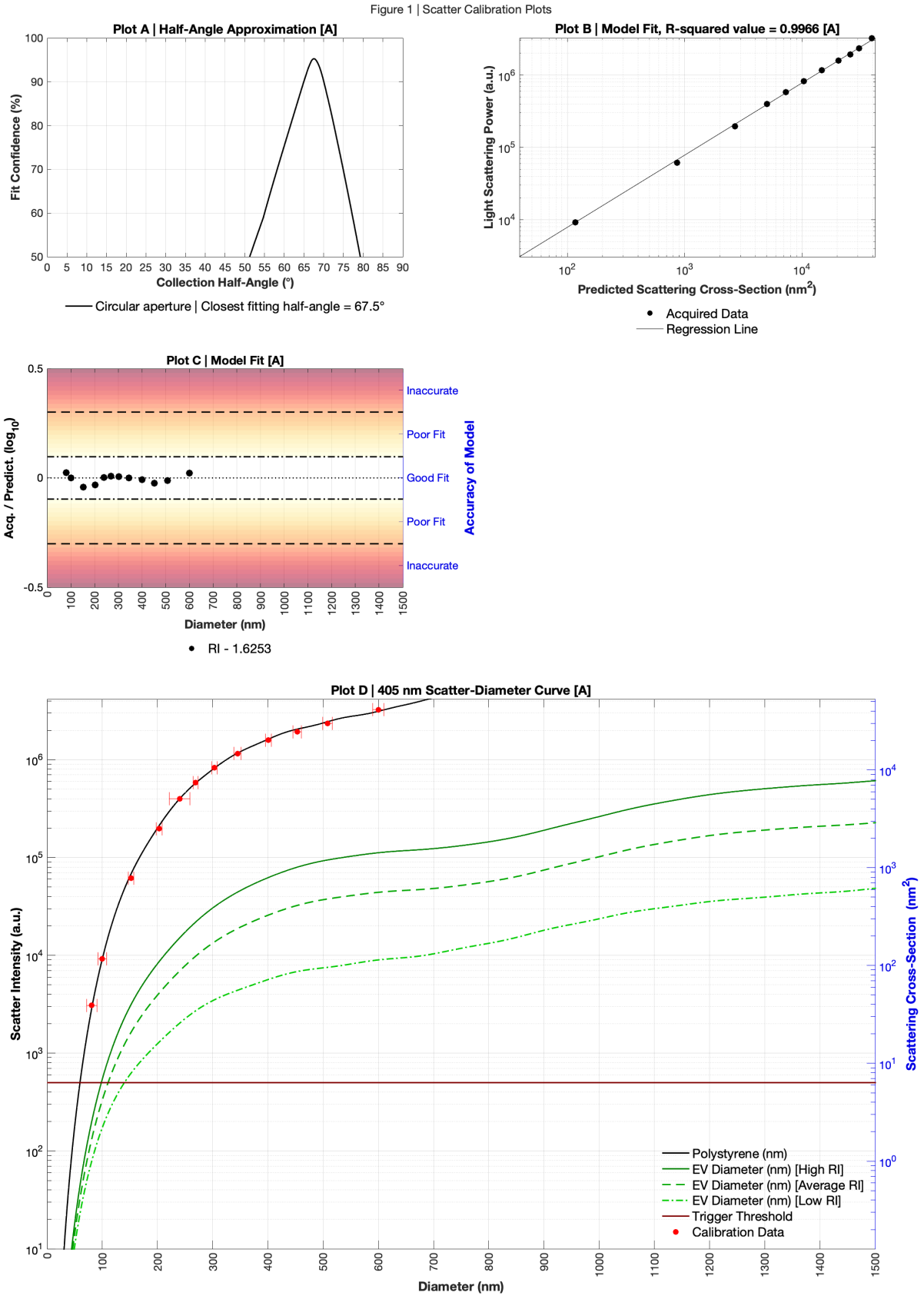

Fig. S2. FCM_{PASS} scatter calibration report for Cytek Aurora

3. Prerequisites of RI derivation using FCM

Scattering cross-section (nm2) is a standard unit used to report light scattering signals detected in FCM. Mie Theory provides the mathematical function to calculate the scattering cross section (nm2) for nanoparticles of known diameter and refractive index (Figure S3A). When the RI of a particle is unknown, this same function can be used to derive the RI, given that diameter and scattering cross-section are known (Figure S3B). Scattering cross-section can similarly be derived if the RI and diameter are defined (Figure S3C). When using scattering cross-section to determine refractive index using flow cytometry, a method of deriving the diameter of a particle must be obtained. This can be achieved by using fluorescence staining or tagging where the fluorescence signal scales with the particle diameter.

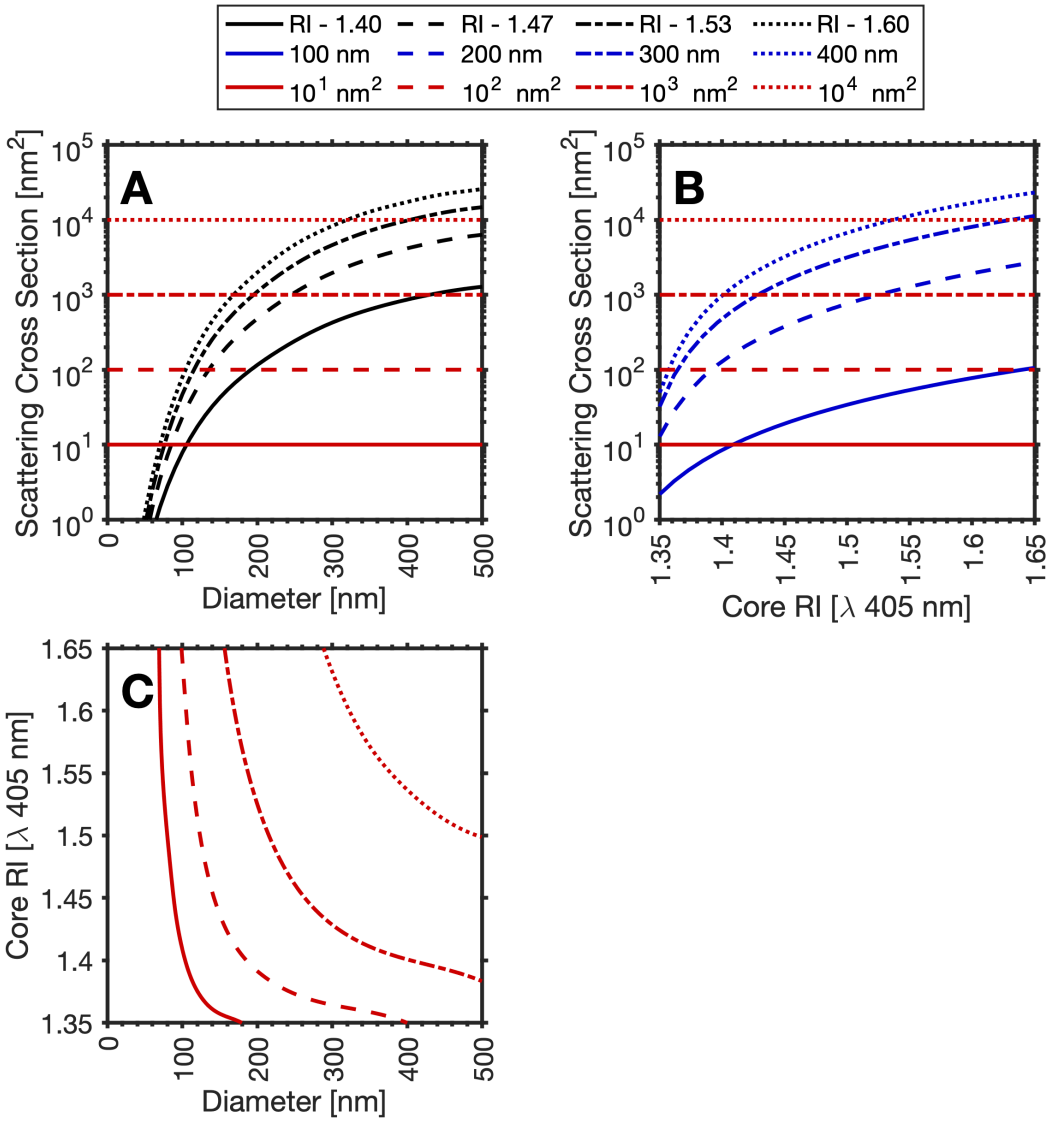

Fig. S3. Example light scattering models using Cytek Aurora collection half-angle. A) Scatter-diameter curve for Cytek Aurora FCM with example curves at RIs of 1.40 (solid black line), 1.47 (dashed black line), 1.53 (dot dash black line), 1.60 (dotted black line). Reference scattering cross sections are shown as horizontal lines at 101 nm2 (solid red line), 102 nm2 (dashed red line), 103 nm2 (dot dash red line), 104 nm2 (dotted red line). B) Scatter-RI curve for Cytek Aurora FCM with example curves at diameters of 100 nm (solid blue line), 200 nm (dashed blue line), 300 nm (dot dash blue line), 400 nm (dotted blue line). Reference scattering cross sections are shown as horizontal lines at 101 nm2 (solid red line), 102 nm2 (dashed red line), 103 nm2 (dot dash red line), 104 nm2 (dotted red line). C) RI-diameter curve for Cytek Aurora FCM with example curves at scattering cross sections of 101 nm2 (solid red line), 102 nm2 (dashed red line), 103 nm2 (dot dash red line), 104 nm2 (dotted red line). All models assume a homogenous sphere models with an illumination wavelength of 405 nm, a circular collection half-angle of 67.5° perpendicular to the illuminating wavelength, and a surround medium RI of 1.343.

4. Refractive index derivation using orthogonal analyses

A. Flow cytometry gating and statistics.

Upon acquiring flow cytometry data of fluorescent particles and calibrating the light scattering intensities using FCM_{PASS} software, particle data is gated from background noise, shown in Figure S4.

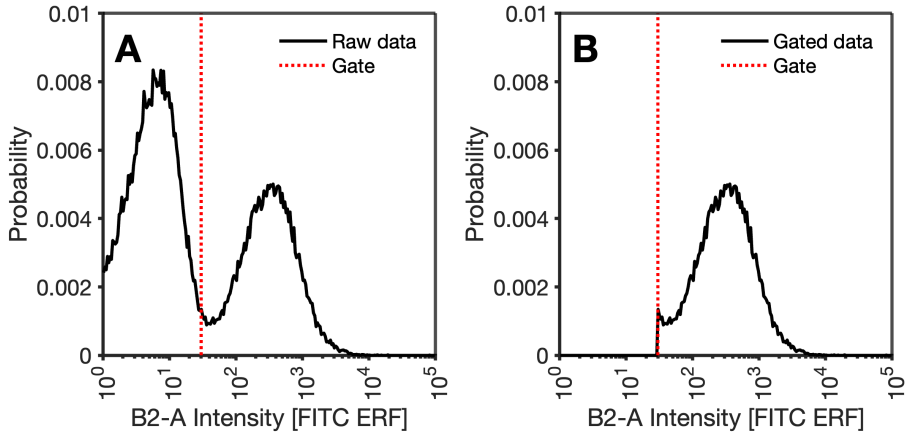

Fig. S4. A) Ungated rEV fluorescent flow cytometry data B) Gated rEV fluorescent flow cytometry data. Red line indicated lower limit of detection that was used to gate fluorescent rEV data.

Once the flow cytometer fluorescence population is gated, this population's intensity is treated as scaling linearly to particle surface area. This population then has a lognormal distribution fitted to it by log transforming the data and fitting a normal distribution. Once this distributing has been derived, the 5th to 95th percentiles of the B2-A intensity / Surface Area are obtained, shown in Figure S5.

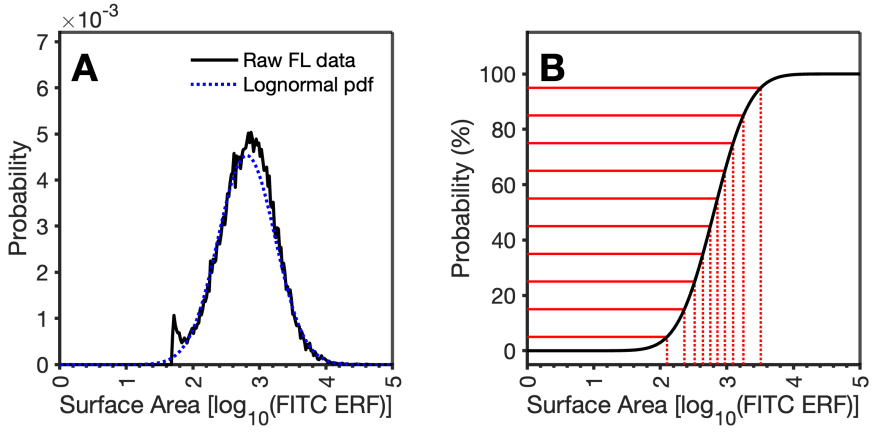

Fig. S5. A) Fitting distribution to flow cytometry data and B) obtaining percentile statistics

B. MRPS gating and statistics.

Next microfluidic resistive pulse sensing (MRPS) data is calibrated using RPS_{PASS} software and exported as .mat files. This data is then gated in order to remove the noise population and the 203 nm spike-in NIST-traceable bead population used for calibration, shown in Figure S6. The gated used had a transit time to signal to noise ratio > 1, and a diameter < 180 nm.

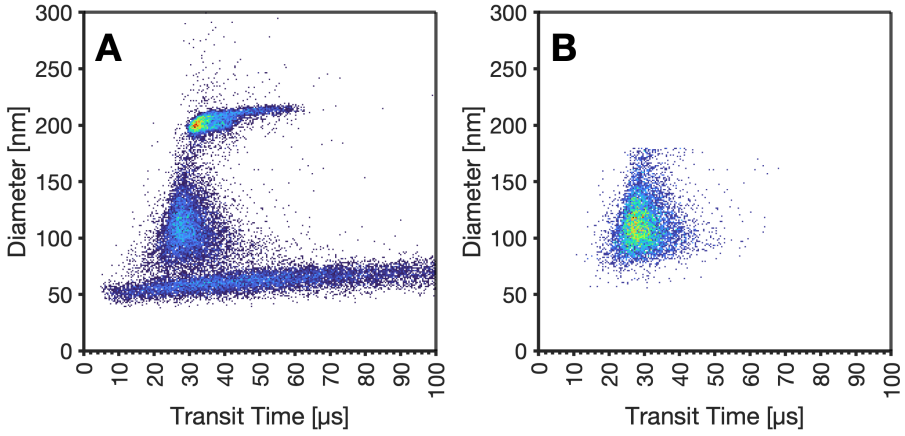

Fig. S6. A) Ungated MRPS rEV data. B) Gated of MRPS rEV data

Once the MRPS population is gated, the diameter measurement is converted surface area using the formula πd^2. This population then has a lognormal distribution fitted to it by log transforming the data and fitting a normal distribution. Once this distributing has been derived, the 5-95th percentiles of the B2-A intensity / Surface Area are obtained in 1 percent increments, shown in Figure S7.

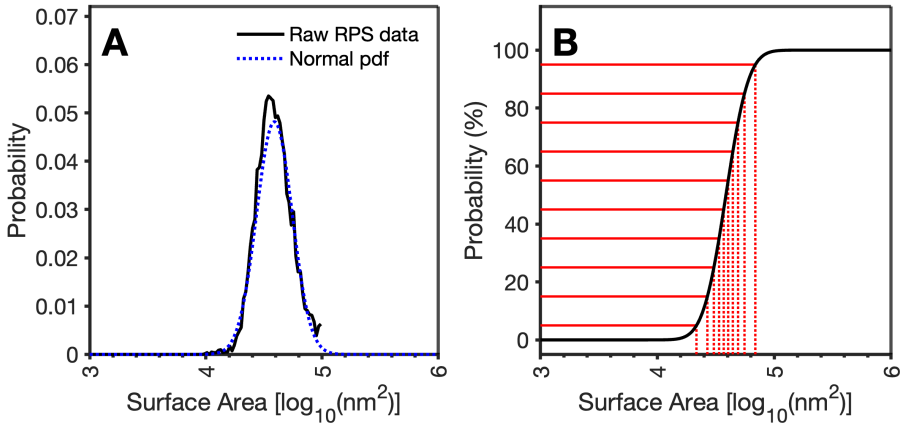

Fig. S7. A) Fitting distribution to MRPS data and B) obtaining percentile statistics

C. Deriving refractive index from single particles.

By obtaining the percentiles of the fitted distributions from flow cytometry and MRPS, it is possible to calibrate the fluorescence surface area data into units of nm^2. This is done by performing a regression of the 5-95th percentiles data once it has been log transformed, as shown in Figure S8A. This regression not only scales the fluorescence data but also the flow cytometry electronics resolution to that of the MRPS data. Therefore the slope of the regression is not expected to equal to 1. Once the flow cytometry data has been scaled to surface area; SA, in units of nm^2, it can then be converted to diameter; d, by using the formula $d = \sqrt{\frac{SA}{\pi}}$. It can be seen that the raw fluorescence data when converted to diameter and compared to the MRPS data is now highly concordant, Figure S8B.

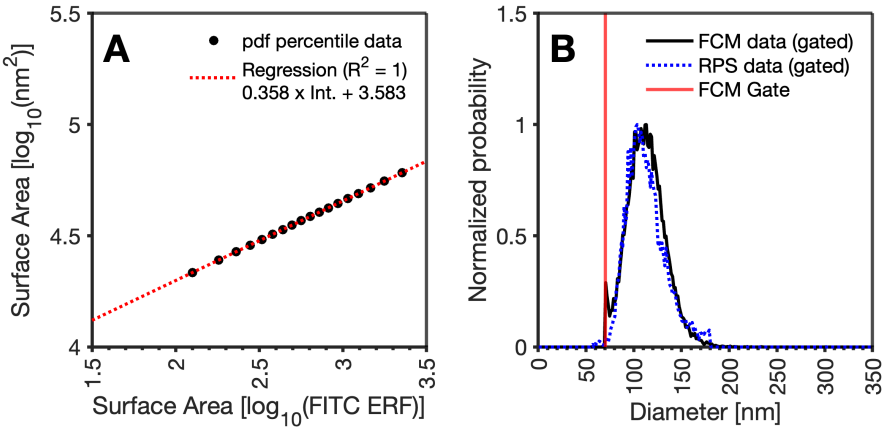

Fig. S8. A) Regression of MRPS vs. flow cytometry surface area. B) Flow cytometry fluorescence derived diameter distribution data (black line) overlaid with MRPS diameter distribution data (blue dotted line). Flow cytometer lower limit of detection indicated with red line.

Upon calibrating the flow cytometry fluorescence data to diameter, all raw data now has a scattering cross-section and a diameter independently associated with every event, Figure S9A. This allows for the diameter versus scattering cross section plots to be used to derive the core refractive index of each particle by interpolating the data with the database generated.

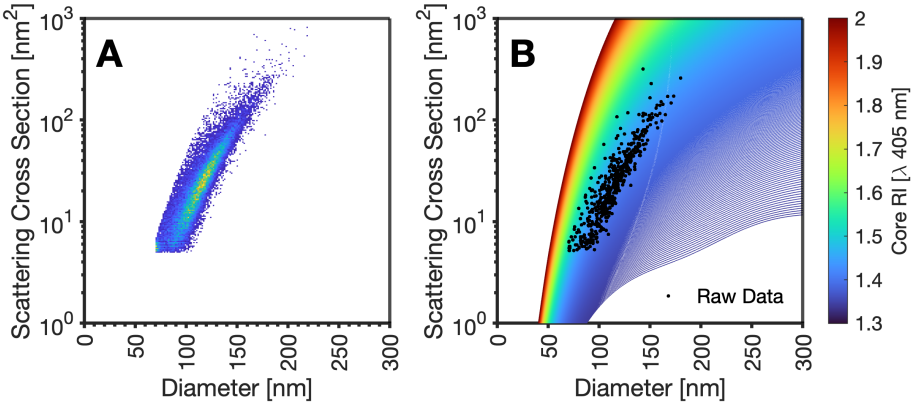

Fig. S9. A) Gated rEV particles. B) Gated rEV particles overlaid with scattering cross section vs. diameter refractive index database

D. Deriving refractive index from a population of particles.

Deriving the refractive index with a population based can be performed with two methods defined in this manuscript as Method 2A and Method 2B. These methods start similarly to Method 1, whereby data is gated to isolate the population being quantified with flow cytometry (Section A) and MRPS (Section B).

Using the collection angle of the calibrated flow cytometer a refractive index database is constructed, Figure S10A, and gated scattering cross section data is obtained, Figure S10B.

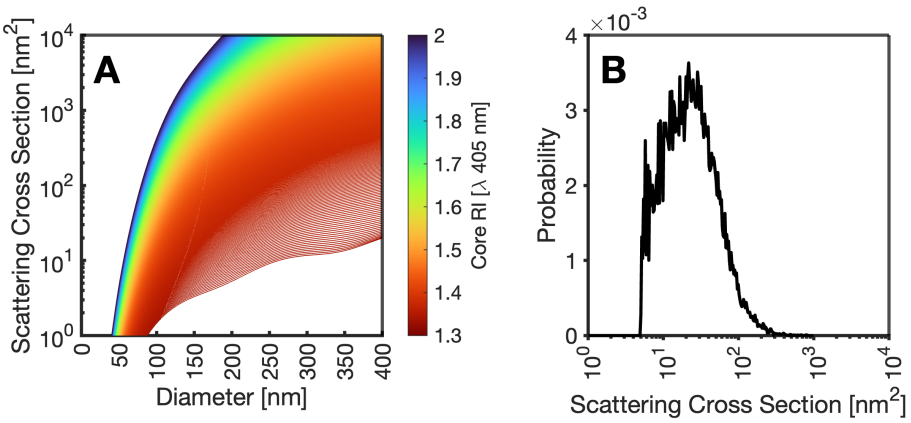

Fig. S10. A) Scattering cross section vs. diameter refractive index database. B) Raw scattering cross section data from flow cytometer.

Flow cytometry scattering cross section data is sequentially interpolated with each reference refractive index in the database to produce a surface area distribution. This data is log10 transformed and has a normal distribution fitted to the data, Figure S11A. MRPS surface area data is also log10 transformed with a normal distribution fitted to the resulting data, Figure S11B.

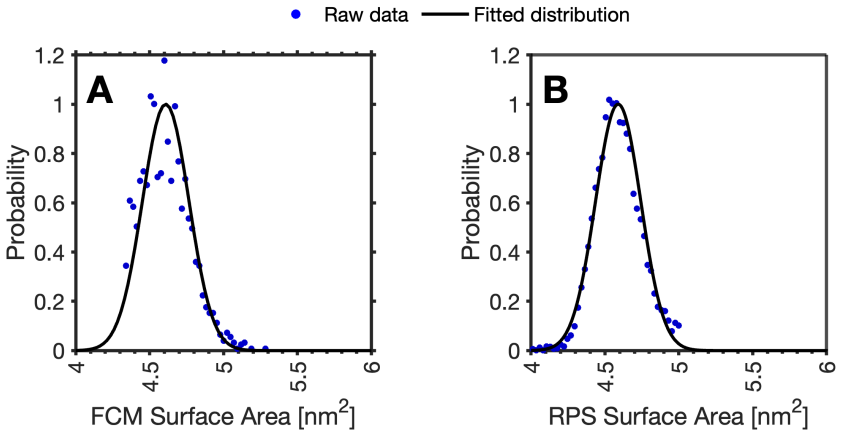

Fig. S11. A) Fitting normal distribution to log transformed surface area data from flow cytometry. B) Fitting normal distribution to log transformed surface area data from MRPS.

The fitted normal distributions are converted to cumulative distribution functions and the 1st to 99th percentile of flow cytometry and MRPS data is obtained, Figure S11.

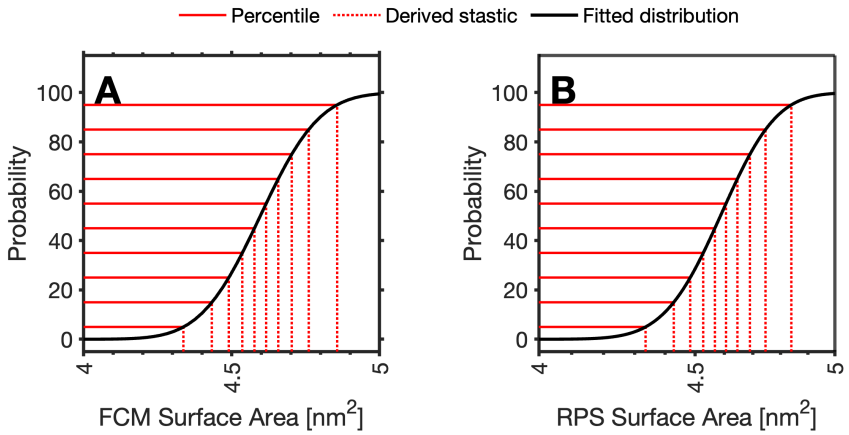

Fig. S12. A) Deriving percentile data from flow cytometry (FCM) surface area distribution. B) Deriving percentile data from MRPS surface area distribution.

A regression is the performed using the percentile data from MRPS and flow cytometry, Figure S13A. With each regression the residual sum of squares (RSS) found by subtracting the known tested diameter distribution percentiles from the flow cytometry data from the known distribution with MRPS percentile data at each refractive index tested, equation 6.

$$RSS = \sum_{i=1}^{n} (MRPS - FCM_i)^2 \quad [6]$$

Once the RSS has been calculated for each refractive index tested, the regression yielding the smallest RSS value is deemed the closest fitting refractive index for the population, Figure S13B.

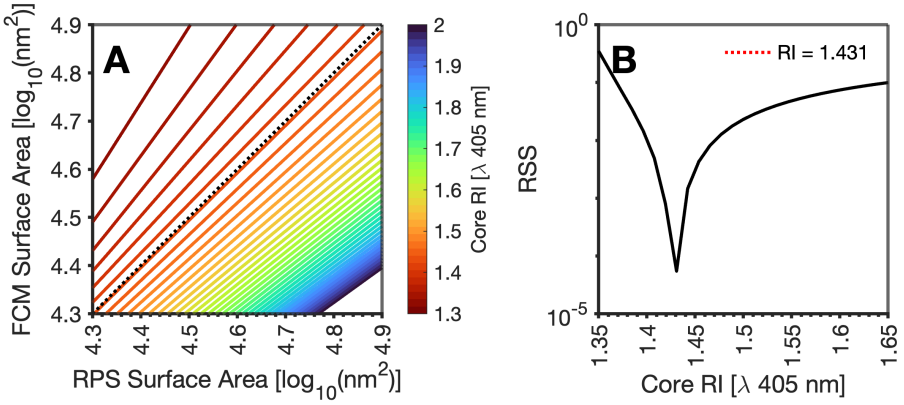

Fig. S13. A) Regression of MRPS vs. flow cytometry surface area. B) Residual sum of squares comparison at each tested refractive index. Closest fitting refractive index indicated by dotted red line.

References

1. M C., Matlab functions for mie scattering and absorption. (2002-11).
2. CF Bohren, DR Huffman, *Absorption and scattering of light by small particles.* (Wiley, New York ; Chichester), (1983).
3. JA Welsh, et al., Fcmpass software aids extracellular vesicle light scatter standardization. *Cytom. A* **97**, 569–581 (2020).